JOURNAL OF MATERIALS SCIENCE 31 (1996) 437–444

Preparation of V/ZrO_2 catalysts by the sol–gel method: physical and structural characterization

M.L. ROJAS-CERVANTES*, A.J. LOPEZ-PEINADO, J. De D. LOPEZ-GONZALEZ
Departamento de Química Inorgánica y Química Técnica, UNED c/Senda del Rey, s/n. Madrid-28040, Spain

F. CARRASCO-MARIN
Departamento de Química Inorgánica, Facultad de Ciencias, Universidad de Granada, Spain

Some zirconia-supported vanadium oxides have been prepared by sol–gel method and characterized by different techniques. The vanadium content exerts an effect on the area and pore-size of precursors and samples calcined. The presence of vanadium also affects the decomposition of precursors into ZrO_2 and to its phase transformation, as well as the formation of fibres, as shown by SEM-EDX. XPS analyses show the presence of two species of vanadium at the surface, V^{5+} and V^{4+}, the percentage of each one depending on the load of vanadium in the catalyst.

1. Introduction

The sol–gel process offers new approaches to the synthesis of metal oxide materials. Starting from molecular precursors, an inorganic network is obtained via hydrolysis and polymerization reactions at low temperature [1]. Each step of the process can be controlled and modified in order to obtain a specific material, with better characteristics – such as higher surface area, superior homogeneity and purity, better microstructural control of metallic particles and narrow pore-size and particle-size distributions – than those obtained by the traditional methods of preparation [2]. One of the applications of the sol–gel method can be found in the field of catalysis. Thus, a supported oxide catalyst can be prepared from a homogeneous solution which includes both the metal precursor and the support precursor. In this way, the sol–gel method has been successfully used in recent works in the preparation of silica- [3] and alumina- [4] supported platinum catalysts and in the synthesis of a promoting ZrO_2 with NaCl, which is very effective in the oxidative coupling of methane [5].

On the other hand, supported vanadium oxides have been studied for a long time as catalysts in several oxidation reactions [6–8] and have recently been the object of new structural and kinetics research [9–11]. Supported vanadia catalysts can also be used in reduction reactions. Thus, Szackas *et al.* [12] have recently reported the use of a zirconia-supported vanadium oxide catalyst in the selective reduction of NO_x with NH_3. The importance of this type of catalyst in such kinds of reactions, together with the advantages obtained in the supported oxide catalyst prepared by the sol–gel process have encouraged us to prepare some zirconia-supported vanadium oxides by this method with different loadings of vanadium.

2. Materials and characterization

The zirconium (IV) propoxide ($(CH_3–CH_2–CH_2O)_4$ Zr) and the vanadyl acetylacetonate (95 wt % purity) were supplied by Aldrich. Ethanol and nitric acid were from Panreac.

Differential thermal analysis (DTA) and thermogravimetric analysis (TGA) were carried out in a Seiko System 320, under a dry air flow of 50 ml min^{-1}, at a heating rate of 5 K min^{-1}. Finely powdered alumina was used as the reference substance. The BET surface areas and the distribution of pore volumes were measured by nitrogen adsorption at 77 K in a Micromeritics ASAP 2000 equipment. The diffraction patterns were measured and evaluated with a Siemens D500 diffractometer, using CuK_α radiation. The texture of the samples was analysed by scanning electron microscopy (SEM-EDX) with a Zeiss DSM-950 microscope, equipped with a system of microanalysis by energy dispersion X-ray, Link QX-2000 (excitation energy of 20 kV and a beryllium window). Infrared spectra of raw and thermally treated samples were recorded in the range 4000–400 cm^{-1} using the KBr pellet technique with a Bomem MB-100 spectrometer. X-ray photoelectronic spectra (XPS) were recorded in a Fisons Escalab 220R spectrometer, equipped with an excitation source of MgK_α and an energy semispheric analyser. The residue pressure in the analysis chamber was maintained under 1.5×10^{-9} torr (1 torr = 133.322 Pa) during data acquisition.

*Author to whom all correspondence should be addressed.

0022–2461

3. Synthesis

The general procedure was as follows. An aqueous solution of HNO_3 was prepared and added dropwise to a reactor containing an ethanolic solution of zirconium (IV) propoxide (PrO) and vanadyl acetylacetonate (AAVO) in the correct proportions under continuous stirring. At the gelling point, the stirring was stopped and the gel was aged for 5 days at room temperature. The residual alcohol was eliminated by distillation. After the ageing step, samples were dried in an oven at 373 K for 16 h and calcined under an air flow of 50 ml min^{-1} at several temperatures for 3 h, using a heating rate of 5 K min^{-1}.

Four samples were prepared with metal vanadium contents of 0.5, 1, 3, and 5 wt %. In all cases, the molar ratios used for the synthesis were $H_2O/PrO = 3.5$, ethanol/PrO = 15 and $HNO_3/PrO = 0.2$. Samples were denoted V/ZrO_2 followed by a number which indicates the weight per cent vanadium content. For comparative purposes, another sample with a vanadium content of 5 wt % was synthesized by the impregnation method. The support (ZrO_2) was prepared by the sol–gel method, as indicated above. After drying at 373 K (16 h) and calcination at 873 K (3 h), it was impregnated with an ethanolic solution of AAVO and the solvent was removed. The sample was dried at 373 K (16 h) and calcined at 873 K (3 h); these were denoted V/ZrO_2 5I.

4. Results and discussion

4.1. Physical characteristics

The BET surface areas (determined by nitrogen adsorption at 77 K) of the dried precursors and the samples calcined at 873 K (previously evacuated at 383 K) are given in Table I, together with the pore volumes and the average pore radius. The areas of the precursors are in the range 315–405 $m^2 g^{-1}$. It was observed that the higher the vanadium content of the sample, the higher was the area of the precursor obtained. This same trend is observed in calcined samples, where the pore structure collapses and the surface area decreases drastically by a factor of around 1/5–1/6. Thus, the samples, which are fundamentally mesoporous, have areas around 50–65 $m^2 g^{-1}$, in contrast to the lowest area value obtained for the sample prepared by impregnation (15.0 $m^2 g^{-1}$). With respect to the pore size, when the vanadium content increases, a decrease of average pore radius occurs, in both precursors and calcined samples. On the other hand, the sample prepared by the impregnation method has an average pore radius of approximately 4.5 times higher than the sample prepared by the sol–gel method, containing the same amount of vanadium. In addition, the pore-size distribution is narrower in the last one, as can be seen in Fig. 1, where the ordinate scale is arbitrary and the pore volume is given by the maximum of each peak. These results confirm the advantage of the sol–gel method with respect to other traditional methods in the preparation of higher area values and narrower pore-size distributions.

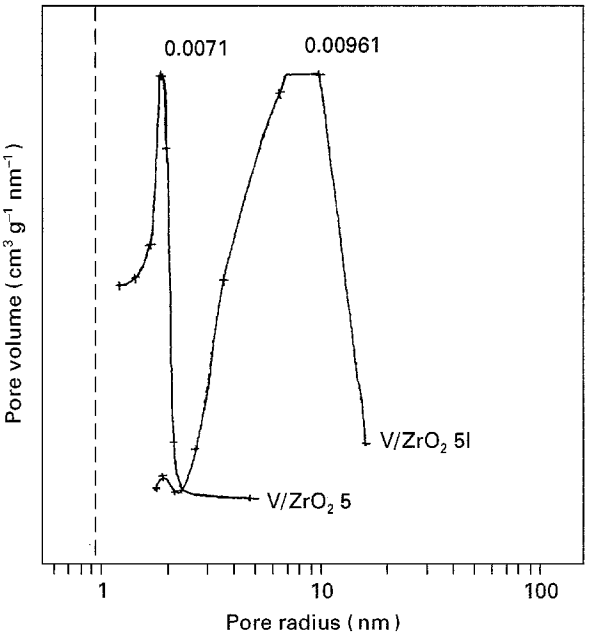

Figure 1 Pore-size distribution of samples containing 5 wt% vanadium prepared by impregnation and sol–gel methods.

4.2. Thermal behaviour

For comparative purposes, and in order to study the weight and energetic changes observed in the thermal analyses of the precursors of V/ZrO_2, TGA and DTA analyses of the PrO and AAVO were also carried out. The TGA and DTA curves for PrO are given in Fig. 2. In the TG curve, a first zone of fast weight loss until around 410 K is observed, which can be assigned to the removal of the propanol present as solvent ($(PrO)_4Zr$ with 30 wt % propanol). On the other hand, the weight loss observed at higher temperatures can be assigned to the removal of the four propoxide groups, leading to the formation of ZrO_2, which remains as a residue. However, the resulting final residue has a value of 31 wt %, which is slightly higher than that corresponding to the complete transformation of the PrO into ZrO_2. This can be the result of the

TABLE I Physical characteristics of dried and calcined samples

Sample	Dried samples (373 K, 16 h)			Calcined samples (873 K, 3 h)		
	S_{BET} ($m^2 g^{-1}$)	V_p ($cm^3 g^{-1}$)	r_p (nm)	S_{BET} ($m^2 g^{-1}$)	V_p ($cm^3 g^{-1}$)	r_p (nm)
V/ZrO_2 0.5	317	0.25	1.57	53.1	0.08	3.00
V/ZrO_2 1	358	0.28	1.54	62.9	0.09	2.96
V/ZrO_2 3	388	0.25	1.28	64.0	0.07	1.68
V/ZrO_2 5	404	0.23	1.15	65.9	0.05	1.54
V/ZrO_2 5I	–	–	–	15.0	0.05	7.10

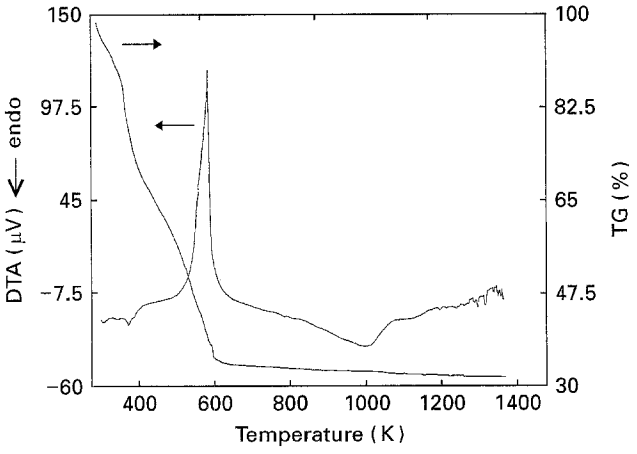

Figure 2 Thermogravimetric and differential thermal analysis curves of zirconium propoxide.

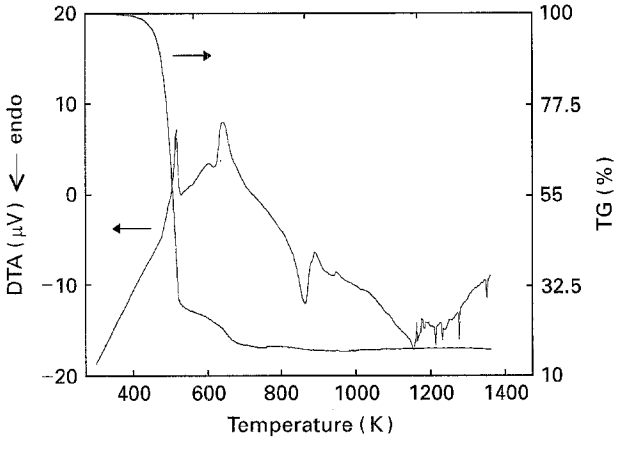

Figure 3 Thermogravimetric and differential thermal analysis curves of vanadyl acetylacetonate.

formation of a carbonaceous residue due to the incomplete removal of the total carbon content of the alkoxide group [13]. The results are slightly different from those reported by us in a recent paper [14], which could be due to the different conditions and system of measurement used. In the DTA curve, an exothermic peak is observed in the temperature range 497–638 K, centred at 593 K, which can correspond to the elimination of the alkoxide groups and to the formation of a crystalline phase of ZrO_2.

The TGA and DTA curves for AAVO are given in Fig. 3. In the TG curve, there is a first zone of fast weight loss until 531 K to give a residue of 27.7 wt %, which agrees well with the removal of the two acetylacetonate molecules, taking into account the 5 wt % impurities of the original AAVO. This weight loss corresponds to an exothermic peak centred at 523 K in the corresponding DTA curve. However, the final residue after heating at 1173 K, has a value of 15.5 wt %, which is smaller than the residue corresponding to a vanadium oxide, in fact even smaller than that corresponding to the metallic vanadium. This fact could be due to the formation of a volatile compound of vanadium or possibly to the melting of vanadium pentoxide, which could spread out in the crucible containing the sample, leading to loss of inorganic material. This can be corroborated by examining the condition

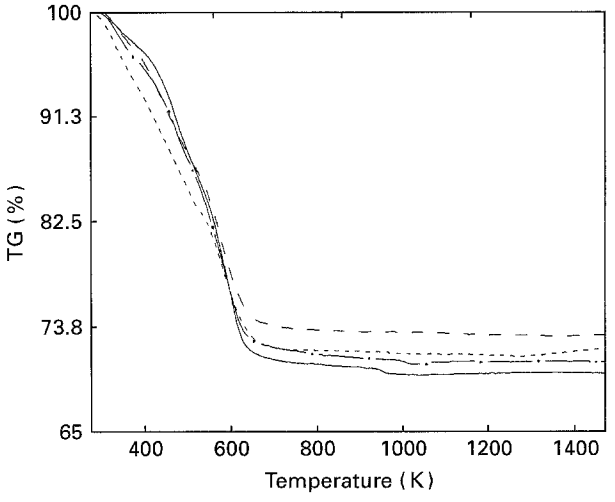

Figure 4 Thermogravimetric analysis curves of samples dried at 373 K. (– – –) V/ZrO_2 0.5; (- - -) V/ZrO_2 1; (–·–) V/ZrO_2 3; (—) V/ZrO_2 5.

of the crucible after the experiment and also by the existence of an endothermic peak centred at a temperature of 863 K, which is near the melting-point temperature of V_2O_5 reported in the literature. There is also another exothermic peak centred at 649 K.

The thermogravimetric analyses of the four samples dried to 373 K are shown in Fig. 4. The complexity of the polymeric system of zirconium–vanadium that can be formed by the hydrolysis makes the assignment difficult of a step in the curve to the removal of a determined component difficult. However, a first zone up to around 518–523 K, can be observed in the derivative curves (not shown in the figure), which could correspond to the decomposition of part of the organic material of AAVO, together with the loss of the physically adsorbed water and alcohol, and to the removal of the propanol of the PrO, although it is not well differentiated in the thermograms. The rest of the curves correspond to the burning of the residual organic material. In all samples, a residue of around 70 wt % is obtained after heating at 1473 K. However, the higher the vanadium content, the higher is the weight loss. Thus, the final weight percentage observed for sample V/ZrO_2 0.5 was found to be 72.8%, compared with 69.5% of the sample V/ZrO_2 5.

The corresponding differential thermal analyses are shown in Fig. 5. The ordinate scale is arbitrary, although all curves have been plotted in the same range of microvolts. The temperatures of the maxima of the peaks observed are given in Table II, together with those corresponding to PrO and AAVO. Three exothermic peaks can be observed in the DTA curves. The first one, located in the temperature range 483–523 K, can be assigned to the decomposition of the organic material of AAVO, and shifts to lower temperatures with increasing vanadium content. The second exothermic peak observed around 583–593 K could be due to the decomposition of the zirconium propoxide present in the sample (the corresponding peak in the DTA curve is observed at 593 K for PrO). The heat evolved in the process associated with these two peaks increases with vanadium content and it is

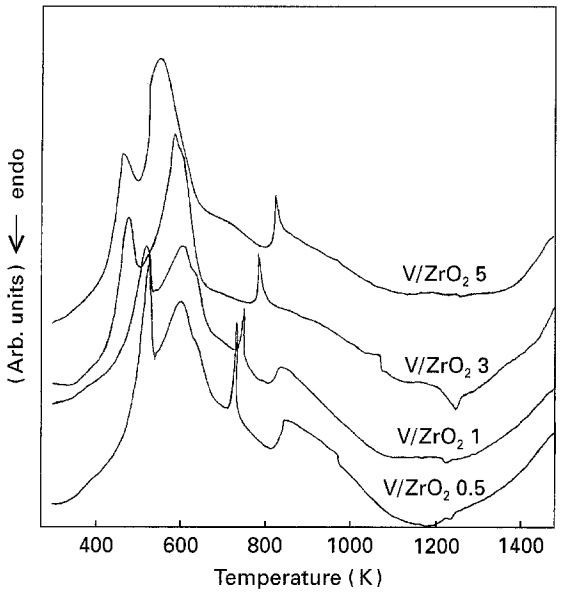

Figure 5 Differential thermal analysis curves of samples dried at 373 K.

TABLE II Temperature of the peak maxima of DTA for samples dried at 373 K and for PrO and AAVO

Sample	T (K) exo				T (K) endo
PrO	–	529.9	–	–	–
AAVO	522.9	–	649	–	863.6
V/ZrO_2 0.5	511.1	589.5	–	721.1	811.8
V/ZrO_2 1	500.0	584.2	–	738.5	808.3
V/ZrO_2 3	488.4	590.2	–	782.1	–
V/ZrO_2 5	483.0	595.7	–	821.3	–

ranges between values of 317.7 cal g^{-1} (where 4.187 cal = 1 Joule) for sample V/ZrO_2 0.5 and 541.1 cal g^{-1} for sample V/ZrO_2 5. There is a third exothermic peak around 723–823 K, with a magnitude of the order of 15–25 cal g^{-1}, which could be associated with the formation of a crystalline phase from the amorphous precursor, because it corresponds to a near constant weight in the corresponding thermogravimetric analysis. This peak shifts to higher temperatures with increasing vanadium content, which seems to indicate that the presence of vanadium retards the formation of the crystalline phase of ZrO_2. Finally, an endothermic peak is observed around 808 K (corresponding to the peak at 863 K observed for AAVO and is due to the melting of V_2O_5) for the two samples of lowest vanadium content. In the other two samples of higher load, this peak is not observed, because it can be masked by the exothermic peak around 823 K.

4.3. Crystalline phases

The temperature of 873 K was chosen to calcine samples, because the TGA curve of the precursors showed constant weight from that temperature, and in the corresponding DTA analyses, no peak was observed at higher temperatures. In order to determine the thermal stability of samples, they were also calcined at two higher temperatures (1073 and 1373 K). X-ray diffractograms of sample V/ZrO_2 3 calcined at the temperatures mentioned are shown in Fig. 6a. In the X-ray diffractogram of sample V/ZrO_2 3 calcined at 873 K the cubic phase of ZrO_2 is observed, in agreement with other authors, who reported that when ZrO_2 is produced by hydrolytic polycondensation of zirconium alkoxides, the initial phase is cubic [14, 15]. This cubic phase converts to monoclinic upon heating, and the diffractogram of the sample calcined at 1073 K shows the presence of the monoclinic phase, which continues present in the diffraction pattern of a sample calcined at 1373 K (there is no phase transformation in this last range of temperatures). However, the cubic to monoclinic phase transformation cannot be associated with an energetic process of any magnitude, because no peak is observed in the corresponding DTA curve in the range 873–1073 K. The phases present in the diffraction patterns for all calcined samples are shown in Table III, together with the average crystal size determined by the Debye–Scherrer equation (from the diffraction peaks (1 1 1) and (1 1 $\bar{1}$) for cubic and monoclinic phases, respectively). The existence of diffraction peaks which can be assigned to vanadium phases is not observed in any case, and this could be due to the fact that with the vanadium contents used in this work, the dispersion of vanadium is such that the crystal size of vanadium oxides formed is not large enough to be detected by XRD. From Table III, it can be seen that an increase in the crystal size occurs with increasing calcination temperature due to the sintering of particles. As an example, the crystal size for sample V/ZrO_2 3 calcined at 1373 K is about four times higher than that of the sample calcined at 873 K. In Fig. 6b the diffractograms of samples calcined at 873 K are given. It is observed that for a vanadium content lower than 3 wt %, the transformation of cubic into monoclinic phase is not completed at 873 K. Thus, in the diffractogram of sample V/ZrO_2 0.5, both phases coexist, and some trace amounts of the cubic phase are still observed in the diffractogram of sample V/ZrO_2 1. For samples V/ZrO_2 3 and V/ZrO_2 5, the only phase present is the monoclinic one. Therefore, although no vanadium phase is detected, the vanadium content affects the cubic to monoclinic phase transformation and the crystallinity of the sample. Thus, the crystal size of ZrO_2 increases with increasing vanadium content. In this way, an average crystal size of around 15.0 nm is observed for samples containing 0.5, 1, and 3 wt %, compared to the 23.0 nm for sample V/ZrO_2 5, all of which were calcined at 873 K. This behaviour is more acute when the calcination temperature is higher. So, the crystal size of V/ZrO_2 0.5 calcined at 1073 K is 18.3 nm, in comparison with the 64.9 nm for sample V/ZrO_2 5 (54.1 nm for sample V/ZrO_2 3).

4.4. XPS results

XP spectra of levels O 1s, V $2p_{3/2}$ and Zr 3d were recorded for samples V/ZrO_2 3 and V/ZrO_2 5, calcined at 873 and 1373 K, as well as for sample V/ZrO_2 3 calcined at 873 K and reduced under a hydrogen flow of 50 ml min^{-1} for 1 h. Previous to the analysis,

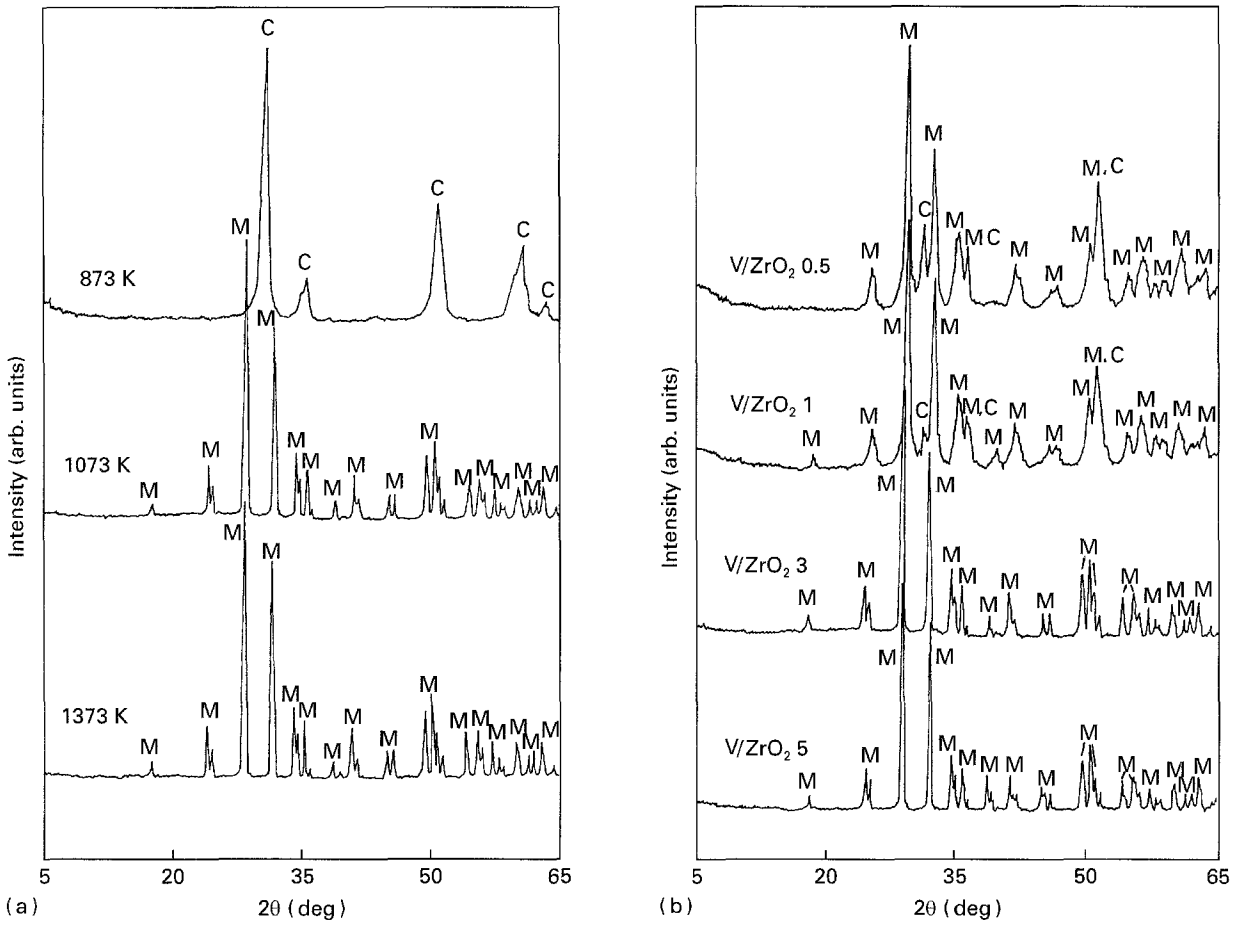

Figure 6 X-ray diffraction patterns of some samples. (a) V/ZrO_2 3 calcined at several temperatures. (b) Samples calcined at 873 K. M, monoclinic phase; C, cubic phase.

TABLE III Crystalline phases and average crystal size for calcined samples

Sample	Crystalline phases			d (nm)[a]		
	873 K	1073 K	1173 K	873 K	1073 K[b]	1373 K
V/ZrO_2 0.5	C	M,C	–	15.5	18.3	–
V/ZrO_2 1	C	M,C	–	14.8	18.0	–
V/ZrO_2 3	C	M	M	15.3	54.1	86.1
V/ZrO_2 5	C	M	M	23.0	64.9	102.4

[a]Crystal size determined by Debye–Scherrer equation; C, ZrO_2 cubic; M, ZrO_2 monoclinic.
[b]Calculated for monoclinic phase.

samples were outgassed in a high vacuum. The binding-energy scale was calibrated with respect to the Zr $3d_{5/2}$ reference signal at 182.5 eV. Binding energies (eV) of levels O 1s and V $2p_{3/2}$, together with the intensity ratios determined by XPS for the samples noted above are given in Table IV. From this table, it can be seen that spectra of level V $2p_{3/2}$ for samples calcined at 873 K show the contribution of two oxidation states, V^{5+} and V^{4+}, with binding energies around 517.7 and 516.5 eV, respectively. The existence of V^{5+} could be due to the bombardment by X-rays, which can lead to the removal of electrons from vanadium. These results agree with those reported by Chiarello *et al.* [16] for titania-supported vanadium catalysts prepared by impregnation and calcined at 693 K. In sample V/ZrO_2 3, the contents of V^{5+} and V^{4+} in the surface are quite similar (44% and 56%, respectively), while the contribution of V^{5+} is higher (70%) than that observed for V^{4+} (30%) in sample V/ZrO_2 5. These results show that the higher the vanadium content, the higher is the average oxidation state at the surface. Samples calcined at 1373 K show the existence of only V^{5+}, taking into account that the calcination treatment is carried out under an air flow. The pretreatment in hydrogen at 823 K causes the reduction of V^{5+} to V^{4+}, as evidenced by the value of binding energy for the reduced sample of V/ZrO_2 3. There is no V^{5+} in this sample at the surface, although its presence in the bulk cannot be excluded, because XPS is a technique which analyses a zone of about 3 nm depth.

O 1s spectra for samples calcined at 873 K show two peaks, at 530.4–530.6 eV of lattice oxygen O^{2-}, and at 531.9–532.5 eV of hydroxyl species [17]. These

TABLE IV Binding energies (eV) of inner electrons and intensity ratios for some samples calculated by XPS. Values in parentheses indicate the percentage of each peak

Sample	O ls	$V_2P_{3/2}$	I_V/I_{Zr}
V/ZrO_2 3, 873 K	530.4(67) 531.9(33)	516.5(56) 517.6(44)	0.066
V/ZrO_2 3, 1373 K	530.6	517.7	0.492
V/ZrO_2 3, 873 K	530.5(75)	516.2	0.065
$T_r = 823$ K	532.0(25)		
V/ZrO_2 5, 873 K	530.6(86) 532.5(14)	516.7(30) 517.7(70)	0.134
V/ZrO_2 5, 1373 K	530.3	517.7	0.466

last species can be formed by the dissociative adsorption of water vapour from the atmosphere. In both samples, the peak placed at lower BE makes a major contribution, although its relative intensity increases in the sample of higher vanadium content, as occurs with the intensity of the peak for the V^{5+} with respect to V^{4+}. The existence of two oxygen peaks is also revealed in the sample reduced in hydrogen. Calcination treatment at higher temperatures leads to a less reactive surface and the peak of hydroxyl species disappears in samples calcined at 1373 K, showing only the existence of lattice oxygen.

With respect to the intensity ratios I_V/I_{Zr}, for samples calcined at 873 K, V/Zr ratios in the surface near to the theoretical one for bulk, 0.075 and 0.128 for V/ZrO_2 3 and V/ZrO_2 5, respectively, are observed. However, the surface of the latter sample is slightly enriched in vanadium. A very important enrichment of vanadium at the surface is produced for samples calcined at 1373 K. In the case of V/ZrO_2 3, the surface is enriched by a factor of 6.5 with respect to the theoretical ratio, and by a factor of 3.5 in sample V/ZrO_2 5. This enrichment could be due to the melting of V_2O_5, which occurs around 873 K and could cause the migration of V_2O_5 from bulk to surface. This leads to a lower dispersion of vanadium at the surface of samples calcined at higher temperatures, which could cause differences of behaviour in the use of these samples as heterogeneous catalysts.

4.5. SEM-EDX results

The grain morphology and aggregation state of V/ZrO_2 samples were characterized by scanning electron microscopy. Fig. 7 shows the evolution of texture with calcination temperature for the sample with a vanadium content of 3 wt %. In the precursor and in the sample calcined at 873 K (Fig. 7a and b, respectively), homogeneous particles with a V/Zr ratio near to the theoretical one are observed (which agrees with XPS results), together with a few particles more clear deposited on them, which contain vanadium (approximately 40 wt %) with a lower concentration of zirconium (around 60 wt %). When the calcination temperature increases, these particles enriched in vanadium disappear and there is a practically homogeneous composition, showing however a global enrichment of

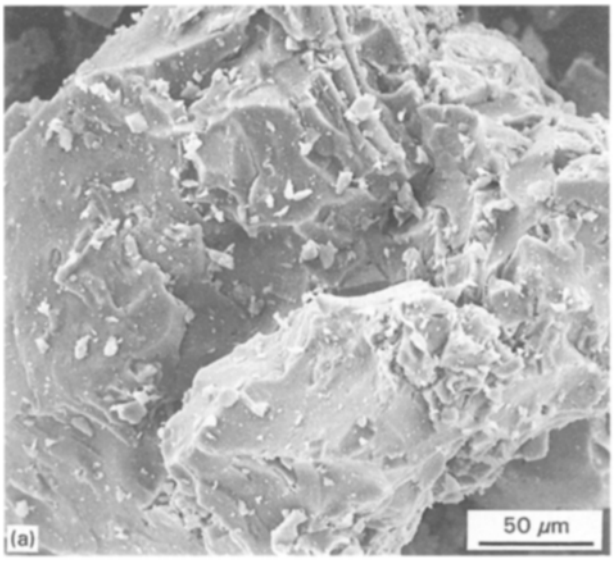

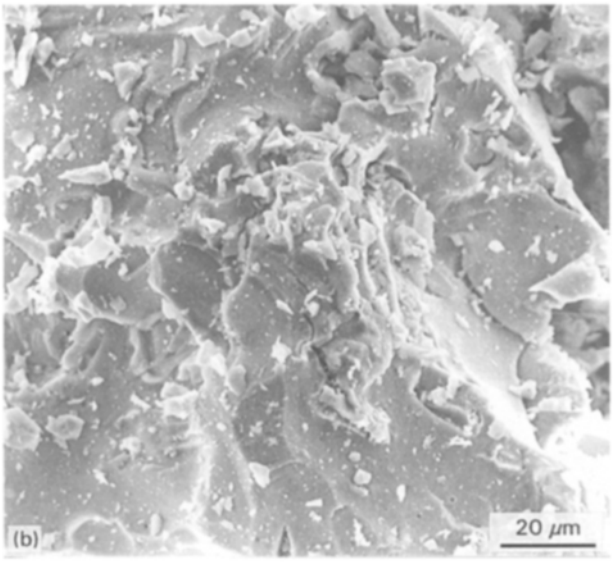

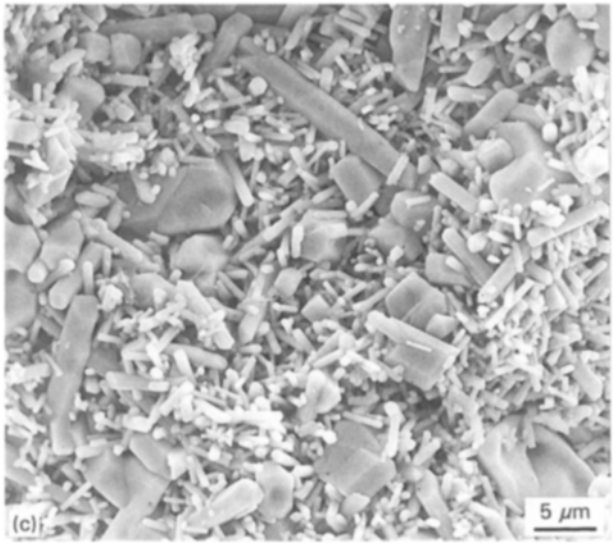

Figure 7 Scanning electron micrographs of samples with a vanadium content of 3 wt%, (a) dried at 373 K, (b) calcined at 873 K and (c) calcined at 1373 K.

vanadium at the surface (which also agrees with the results found by XPS). In addition, the morphology changes and particles appear as agglomerates of granules and sintered fibres (see Fig. 7c of sample

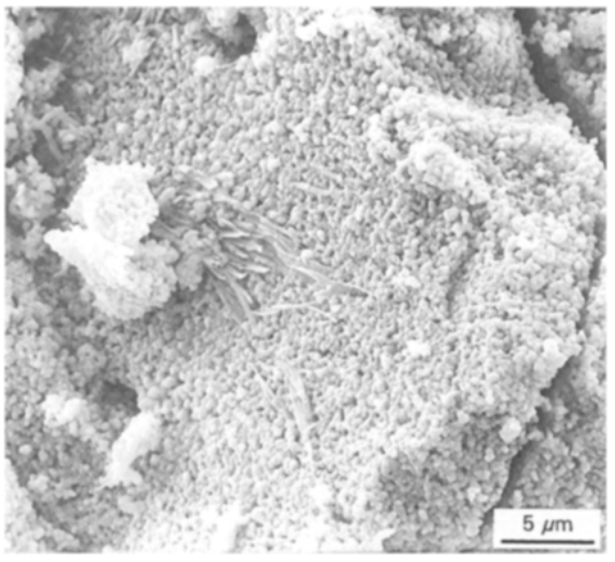

Figure 8 Scanning electron micrograph of sample V/ZrO_2 calcined at 1073 K.

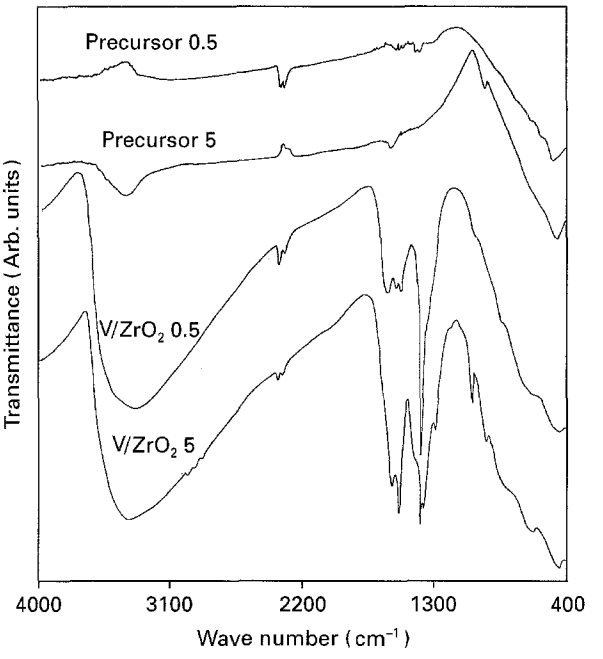

Figure 9 Infrared spectra of some precursors and samples calcined at 873 K.

V/ZrO_2 3 calcined at 1373 K). When the vanadium content increases, the formation of fibres occurs at a lower temperature. Thus, in sample V/ZrO_2 5, calcined at 1073 K (Fig. 8), the coexistence of fibres and microparticles can be already observed.

4.6. Infrared results

Infrared spectra of precursors dried at 373 K and oxide samples calcined at 873 K of samples containing 0.5 and 5 wt % are shown in Fig. 9. Band positions and assignments are given in Table V.

The broad band centred at 3450–3350 cm^{-1} is the result of vibration of adsorbed water or structural OH. On the other hand, in the spectra of precursors there is a series of bands which disappear in calcined samples. For example, the three bands around 2900 cm^{-1} are characteristic of the vibration of methyl groups of acetylacetonate compounds [18]. These bands do not exist in the precursor of sample V/ZrO_2 0.5, probably due to the lower vanadyl acetylacetonate content. Other bands, assigned to vibration modes of CH_3 groups, are located at around 1430, 1385, and 1360 cm^{-1}, also disappear in calcined samples. The band around 1627 cm^{-1}, which appears in the precursor of V/ZrO_2 0.5 and in calcined V/ZrO_2 5, could be due to the deformation mode of adsorbed water. Bands around 1570 and 1530 cm^{-1} are assigned to a combination of vibration modes of C–C and C–O groups in acetylacetonate, and they are much more intense in the sample with higher vanadium content. They do not appear in the spectra of

TABLE V Infrared bands for some samples (wave numbers in cm^{-1})

Group[a]	Dried samples (373 K, 16 h)		Calcined samples (873 K, 16 h)	
	V/ZrO_2 0.5	V/ZrO_2 5	V/ZrO_2 0.5	V/ZrO_2 5
υ(O–H)	3351	3373	–	3432
δ(O–H)	1627	–	–	1626
$\upsilon(CH_3)$	–	2970, 2934, 2877	–	–
$\delta_d(CH_3)$	–	1429	–	–
$\delta_s(CH_3)$	1385, 1357	1383, 1362	–	–
?	–	1283	–	–
HCOO	–	–	1580, 1345	–
υ(C–C) + υ(C–O)	1573, 1539	1577, 1532	–	–
υ(V=O)	–	1031, 933	–	993
?	834	–	–	–
π(CH)	–	788	–	–
$\pi(CH_3\text{-}C\lesssim^{C}_{O})$ or Zr-O(ZrO_8)	642	637	–	–
V-O(V^{4+})	–	–	668	–
?	–	–	581	–
?	–	–	495	478
$\upsilon(MO) + \upsilon(C\text{–}CH_3)$ or Zr–O(ZrO_8)	439	429	–	–

[a]υ, stretching; δ, in-plane bending or deformation; π, out-of-plane bending; s, symmetric; d, degenerate.

calcined samples. Bands around 640 cm^{-1} could be due to the vibration of group $CH_3-C\langle^{C}_{O}$ or to Zr–O in ZrO_8 groups. Finally, bands around 440–430 cm^{-1} could be a combination of vibration modes of MO (M = metal) and C–CH_3 or due also to vibrations of Zr–O in ZrO_8 groups [18, 19].

In the sample V/ZrO_2 5 calcined at 873 K, a band centred at 993 cm^{-1} appears, which is assigned to the stretching of V=O of V_2O_5 formed in the calcination process. In general, in hydrated samples, the stretching of V=O causes a band at that wave number. The hydration of sample V/ZrO_2 5 calcined at 873 K is also confirmed by the presence of a band at 1626 cm^{-1}. This band does not exist in the sample with a lower vanadium content. In it, a band at 668 cm^{-1} appears, which could be due to the vibration of V–O of VO_2. By XPS it was observed that when the vanadium content of the sample decreased, the amount of V^{4+} at the surface increased. Thus, the existence of less V^{5+} and more V^{4+} in the sample V/ZrO_2 0.5 can also be corroborated by the Fourier transform–infrared (FT–IR) bands observed. In this calcined sample, there are, in addition, three bands, two at 1588 and 1345 cm^{-1}, assigned to stretching vibrations of the formate group, asymmetric and symmetric, respectively [20], and another at 1435 cm^{-1}, unassigned. There are some bands, shown in the table, which could not be assigned.

5. Conclusion

Zirconia-supported vanadium oxides have been prepared by the sol–gel method. The vanadium content has an effect on surface area and pore size of the samples obtained. Thus, the higher the vanadium content, the higher the area and the smaller the average pore radius. In addition, samples prepared by the sol–gel method have higher area values and narrower pore-size distributions than those obtained by the classical impregnation method. The presence of vanadium also affects the decomposition of precursors to obtain ZrO_2, because in the DTA curves a shift at higher temperatures of the exothermic peak around 723 K can be seen when the vanadium content increases. By XRD, cubic phase ZrO_2 was detected at 873 K, which converts to monoclinic on heating at 1073 K, the degree of transformation depending on the vanadium content of the samples. As no vanadium phase was detected by XRD, its presence was studied by XPS. Samples calcined at 873 K show the existence of two species of vanadium, V^{4+} and V^{5+} at the surface; the content of V^{5+} increases with increasing vanadium content in the sample. Samples calcined at 1373 K show only the existence of V^{5+} at the surface, and a very important enrichment of vanadium, due probably to the migration of V_2O_5 from bulk to surface, leading to a lower dispersion of vanadium. An increase in the calcination temperature leads to the formation of fibres, which appear at lower temperatures when the vanadium content increases. The decomposition process of precursors to oxides was followed by the FT–IR technique. Infrared spectra of precursors show a series of bands which disappear on calcination.

Acknowledgement

We thank Professor José Luis García Fierro for the XPS measurements and discussion, and to Dr. Miguel Angel Vincente Rodriguez for the XRD measurements.

References

1. B. J. J. ZELINSKY and D. R. UHLMANN, *J. Phys. Chem. Solids* **45** (1984) 1069.
2. C. SANCHEZ and J. LIVAGE, *New J. Chem.* **14** (1990) 513.
3. T. LOPEZ, A. ROMERO and R. GOMEZ, *J. Non-Cryst. Solids* **127** (1991) 105.
4. K. BALAKRISHNAN and R. D. GONZALEZ, *J. Catal.* **144** (1993) 395.
5. A. Z. KHAN and E. RUCKENSTEIN, *Appl. Catal.* **90** (1992) 199.
6. G. C. BOND and S. F. TAHIR, *ibid.* **71** (1991) 1.
7. P. J. GELLINGS, in "Specialist Periodical Reports–Catalysis", Vol. 7, edited by G.C. Bond and G. Webb, (Royal Society of Chemistry, London, 1985) p. 105.
8. S. T. OYAMA and G. A. SOMORJAI, *J. Phys. Chem.* **94** (1990) 5022.
9. M. G. NOBBENHUIS, P. HUG, T. MALLAT and A. BAIKER, *Appl. Catal.* **108** (1994) 241.
10. G. CENTI, E. GIAMELLO, D. PINELLI and F. TRIFIRO, *J. Catal.* **130** (1991) 220.
11. P. G. PRIES DE OLIVEIRA, J. G. EON and J. C. VOLTA, *ibid.* **137** (1992) 257.
12. S. SZAKACS, G. J. ALTENA, T. FRANSEN, J. G. VAN OMMEN and J. R. H. ROSS, *Catal. Today* **16** (1993) 237.
13. R. C. MEHROTRA, in "Sol-Gel Science and Technology", Proceedings of the Winter School on Glasses and Ceramics from Gels, edited by M. A. Aeger, M. Jr. Jafelicci, D. F. Souza and E. E. Zanotto (Sao Carlos, SP, 1989) p.1.
14. M. L. ROJAS-CERVANTES, R. M. MARTÍN-ARANDA, A. J. LÓPEZ-PEINADO and J. de D. LÓPEZ-GONZÁLEZ, *J. Mater. Sci.* **29** (1994) 3743.
15. B. E. YOLDAS, *J. Am. Ceram. Soc.* **65** (1982) 387.
16. G. CHIARELLO, D. ROBBA, G. de MICHELE and F. PARMIGIANI, *Appl. Surf. Sci.* **64** (1993) 91.
17. C. D. WAGNER, W. M. RIGGS, L. E. DAVIS, J. M. MOULDER and G. E. MUILENBERG, "Handbook of X-ray Photoelectron Spectroscopy" (Perkin-Elmer Corporation, Physical Electronic Division, Eden Prairie, 1979).
18. K. NAKAMOTO, "Infrared and Raman Spectra of Inorganic and Coordination Compounds", 4th Edn. (Wiley Interscience, New York, 1986) p. 260.
19. G. MONROS, J. CARDA, M.A. TENA, P. ESCRIBANO and J. ALARCON, *J. Mater. Sci.* **27** (1992) 351.
20. M. Y. HE and J. G. EKERDT, *J. Catal.* **87** (1984) 381.

Received 23 August 1994
and accepted 22 June 1995